Space Environment (Natural and Induced)

Myung-Hee Y. Kim, Ph.D., Senior Scientist, Radiation Biophysics Laboratory, Wyle Laboratories

Kerry A. George, Section Lead, Radiation Biophysics Laboratory, Wyle Laboratories

Francis A. Cucinotta, Ph.D., NASA Chief Scientist, NASA Space Radiation Program

1.5 Radiation

1.5.1 Ionizing Radiation

1.5.1.1 Sources of Ionizing Radiation

Cosmic rays have been studied for a long time and there are many references of their characteristics (Haffner 1967; Ginzburg 1958; Colgate et al. 1963; Meyer 1969). During the last 5 decades, a new field of nuclear science, perhaps "radiation bioastronautics" for the most descriptive way, has been emerging. Cosmic rays, which have extraordinary penetrating power and fall continuously upon the Earth from somewhere beyond, can be the major radiation hazard in manned space missions. Still, there are many challenges of ensuring the proper protection against space radiation hazard for the implementation of NASA's Vision for Space Exploration.

The origin of most cosmic rays is probably in our galaxy, especially in supernova explosions (Ginzburg 1958; Colgate et al. 1963), although the highest-energy components ($\geq 10^{17}$ eV amu^{-1}) may well be of extragalactic origin (Meyer 1969). The Sun contributes significantly to the flux of low energy cosmic rays (below 0.5 GeV amu^{-1}) arriving at the Earth. Disturbed regions on the Sun sporadically emit bursts of energetic charged particles into interplanetary space.

The types and energies of particle radiations in space are summarized in figure 1.5.1.1. The predominant types of particle radiations in the Earth's environment are solar wind protons, auroral electrons, solar storm protons, trapped protons, trapped electrons, solar protons, and galactic cosmic rays (GCRs). There are temporal variations as well as spatial distributions. It is convenient to consider the particulate radiation in space as arising from the distinct sources defined by their location: the solar particle radiation, the galactic cosmic radiation, and the trapped particle radiation.

[figure 1.5.1.1 here]

a) Solar Particle Radiation

The solar wind is really an extension of the solar corona, and extends to at least several astronomical units (1 AU $\approx 1.5 \times 10^8$ km). The solar wind is plasma of both positive and negative particles trapped in a magnetic field emanating from the Sun. It is composed mostly of protons and is persistent through variable parts of the quiet Sun's output. The solar wind protons have thermal energies of ~1 – 10 keV. Except when the Sun is active, the solar wind constitutes the most important particulate solar radiation.

A solar flare is an intense local brightening on the face of the Sun close to a sunspot. The solar abnormality results in an alteration of the general outflow of solar plasma at moderate energies, and in local solar magnetic fields which are carried by that plasma. As the solar plasma envelops the Earth, the magnetic screening effects inherent in plasmas act to shield the Earth from GCR known as a Forbush decrease (Forbush 1937), while contributing far more radiation of their own. When the solar plasma interacts with the geomagnetic field a disturbance or storm occurs. During an intense magnetic disturbance, the Earth's magnetic fields (Van Allen radiation belts) are compressed into the Earth's atmosphere in polar regions

and trapped electrons in the belt are lost. These auroral electrons are seen only in polar regions associated with coronal mass ejection (CME) after solar flares.

The solar protons tend to be eliminated from equatorial regions of the magnetosphere as they are deflected by the horizontal geomagnetic field lines into space. However, solar primary particles arrive at the poles by moving along the near vertical geomagnetic field lines and are thus not deflected. When the low-energy solar storm protons are channelled into the polar regions by the Earth's magnetic field, radio blackouts are produced in the lowest ionospheric region following certain solar flares, which is called a polar cap absorption (PCA) event (Kundu and Haddock 1960).

The radiations with energies below 100 keV – such as solar wind protons and auroral electrons – and the solar storm protons with energies below 10 MeV are considered biologically unimportant since they are shielded against by even gaseous barriers.

In association with many of the optical flares occurring from time to time on the solar surface, large fluxes of solar energetic particles are sometimes accelerated and emitted, and these emissions of solar cosmic radiation are designated solar particle events (SPEs). SPEs with periods of several hours to days represent one of several short-lived manifestations of the active Sun. The solar wind and SPEs are composed of the same types of particles, mostly protons and with the next significant component being alpha particles (Freier 1963; Biswas et al. 1963; Biswas et al. 1962). These two groups of particles are distinguished by their numbers and speeds (energy). Heavier nuclei, mostly in the carbon, nitrogen, and oxygen group (Biswas et al. 1966; Durgaprasad et al. 1968), and even heavier particles (atomic charge number, Z, between 22 and 30) (Bertsch et al. 1969) have also been observed from major SPEs. Rare clusters of high intensity (several orders of magnitude) and high energy events are critical to spaceflight and extravehicular activity (EVA), because the large events

alone determine the yearly fluences of solar particles and there is much higher dose rate effect during a short period of peak (Kim et al. 2006a).

For the past solar cycles 19-21 (1955-1986), the list of major SPEs and the proton fluences are assembled by Shea and Smart (1990), where all the available flux and fluence data are contained in the form of useful continuous database. From 1986 to the present (solar cycles 22 and 23), a SPE list and the GOES spacecraft measurements of the 5-min average integral proton flux are obtained through direct access to NOAA's National Geophysical Data Center (NGDC). Table 1 lists the large SPEs for the past five solar cycles, where the omnidirectional proton fluence with energy above 30 MeV, Φ_{30}, exceeds 10^9 protons/cm^2.

[table 1.5.1.1 here]

Frequency of SPE occurrence recorded by NOAA's GOES satellites is shown in figure 1.5.1.2 within 3-months periods for the solar cycle 23. Here, monthly mean sunspot numbers are included in the figure to show the association between SPE occurrence and solar activity, and the occurrence times of 5 large SPEs are marked with arrows for the criteria having $\Phi_{30} > 10^9$ protons/cm^2. It has been shown an increase in SPE occurrence with increasing solar activity; however, no recognizable pattern has been identified. Large events have definitely occurred during solar active years, but have not occurred exactly during months of solar maximal activity. Moreover, they are more likely to occur in the ascending or declining phases of the solar cycle (Goswami et al. 1988). This sporadic behavior of SPE occurrence is a major operational problem in planning for Moon and Mars missions.

[figure 1.5.1.2 here]

The shapes of the energy spectra as well as the total fluences vary considerably from event to event (Biswas et al. 1962; Freier and Webber 1963; King 1972; Kim et al. 2006b; Shea and

Smart 1990; NGDC 2006). Figure 1.5.1.3 shows the energy spectra of the most recent event of January 16, 2005 SPE. There was a sudden increase in proton flux especially for particles with energies greater than 50 MeV. Protons with energies greater than 100 MeV were increased by as much as four orders of magnitude after having declined from the major pulse. Although during this sharp commencement the fluence did not reach the value obtained at the major peak intensities, this sudden increase of high energy particles may pose more threat than the major particle intensities. Total fluence of an SPE is the representative indicator of a large SPE, and the detailed energy spectra for a large SPE, especially at high energies, is the important parameter for radiation exposure risk assessment (Kim et al. 2006a).

[figure 1.5.1.3 here]

One example of detailed temporal analysis of dose rate at blood forming organ (BFO) is given in the figure 1.5.1.4a for the August 1972 SPE, which is one of large SPEs in modern era and has the highest dose rate at peak. During the peak times, rather heavy shielding (up to 30 g/cm^2 of aluminium) provided by spacecraft is not enough to reduce the BFO dose rate to 1 cGy-Eq/h, where a pivotal transition from low to high dose rates would be started. The temporal behavior shown in this figure suggests significant biological damage would be incurred during the first major peak times. It is noted that biological effects are expected to increase significantly for dose rates above 5 cGy/h. The current recommended 30-day exposure limit at BFO, 25 cGy-Eq (NCRP 2000), is easily exceeded, and early effects from acute exposure may not be avoided when only conventional amount of spacecraft material is provided in order to protect BFO from this class of SPE as shown in figure 1.5.1.4b. To avoid placing unrealistic mass on a space vehicle and at the same time to increase safety factors for astronauts, one shielding solution against SPE would be the selection of optimal vehicle/shielding materials, since it has been shown that materials with lower atomic mass constituents have better shielding effectiveness (Wilson et al. 1995; Cucinotta et al. 2000).

[figure 1.5.1.4a here]

[figure 1.5.1.4b here]

An event of special interest occurred on February 23, 1956 (Wilson et al. 1999) where a striking feature was a large number of high-energy particles early in the event. However, there is still debate on the accuracy of spectral determinations for this event because only ground-based neutron monitors were available. Large uncertainties exist in the determination of spectra due to atmospheric propagation calculations that is required to unfold the spectra. The overall exposure levels from this specific event have been estimated greater than 10 cSv (10 rem) at sensitive sites, while those from other large SPEs recorded in modern era can be reduced below 10 cSv, when heavily shielded "storm shelters" are added to a typical spacecraft (Kim et al. 2005). However, this result should come with the caveat of significant uncertainties in the determination of the source spectra of protons.

b) Galactic Cosmic Radiation

In addition to the radiation from the Sun, the Earth also is bombarded with charged particles from outside the solar system i.e. GCR. These particles appear to pervade at least the near-Earth environment isotropically, and have a range of energies that exceeds 10 GeV per nucleon. GCR is fully ionized nuclei. The electrons are stripped from the atoms during the acceleration to GCR energies. The region outside the solar system in the outer part of the galaxy is believed to be filled uniformly with GCR. The GCR nuclei constitute approximately one-third of energy density of the interstellar medium and, on a galactic scale, they form a relativistic gas whose pressure is important to take into account in the dynamics of galactic magnetic fields. The galactic cosmic ray nuclei are the only direct and measurable sample of matter from outside the solar system. It is a unique sample since it includes all of the elements from hydrogen to the actinides. The GCR arriving beyond the Earth's magnetic field at the

distance of the Earth from the Sun (i.e., 1 AU) is composed of ~ 98 % nuclei and ~ 2 % electrons and positrons (Simpson 1983). In the energy range $10^8 - 10^{10}$ eV amu^{-1}, where it has its highest intensity, the nuclear component consists roughly of 87 % protons, ~ 12 % helium nuclei and a total of ~ 1 % for all of the heavier nuclei from carbon to the actinides (Simpson 1983).

At 1 AU, the GCR flux is affected by solar activity due to interaction with the solar plasma emitted into the interplanetary space, and is out of phase with the Sun's activity – the more active the Sun, the smaller the GCR flux at the Earth. The intensity of the GCR flux varies over the approximately 11-year solar cycle due to the changes in the interplanetary plasma resulting from the expanding solar corona (Bobcock 1961; Badhwar and O'Neill 1992). The GCR flux reaching Earth is decreased during intense sunspot activity, because the low-energy GCR particles are deflected by the Sun's enhanced magnetic field carried by the expanding solar plasma. The maximum dose received occurs at solar minima due to the lower solar plasma output. Measurements at solar minimum modulation, in which major SPEs are usually absent, show the greatest extent of GCR exposure (Badhwar 1999).

GCR has turned out to be a vital contributor to our understanding of high energy phenomena in our galaxy. While protons carry most of the GCR energy, heavy particles give information on composition and propagation. Although GCRs probably include every natural element, not all are important for space radiation protection purposes. The elemental abundances for species heavier than iron (atomic charge number, $Z > 26$) are typically 2 to 4 orders of magnitude smaller than that for iron (Adams et al. 1981). In the solar system some elements such as the L nuclei (Li, Be, B), F and several nuclei between Si and Fe are quite rare (Simpson 1983b; Cucinotta et al. 2006b), whereas in the GCR flux these nuclei are present nearly as commonly as their neighbors (Simpson 1983b). This shows that their origin is in the breakup of heavy particles during GCR propagation which would not be present in the GCR at stellar sources (Parker 1965; Webber et al. 1990a; Fields et al. 1994).

Experimental studies of high-charge and high-energy particles (HZE) were made on the Pioneer, Voyager, and Ulysses spacecraft for the measurements of isotopic composition of GCR elements for near-Earth or deep space (Hesse et al. 1991; Lukasiak et al. 1993, 1995; Webber et al. 1985, 1990a; Wiedenback and Greiner 1981; Wiedenback 1985). These data have been implemented to the development of predictive GCR spectra behind shielding as an important goal for NASA's Space Radiation Research Program (Cucinotta et al. 2006b). Examples of the GCR energy spectra for hydrogen and helium isotopes are shown in figure 1.5.1.5a at solar minimum and solar maximum, and for Ne, Si, and Fe isotopes in figure 1.5.1.5b at solar minimum. These figures show the contribution of different isotopes to primary GCR composition (Cucinotta et al. 2006b). In recent years, new data of the GCR near Mars were collected by MARIE (The Martian Radiation Environment Experiment) on the Mars Odyssey spacecraft (Zeitlin et al. 2004) in order to plan the design of future manned spacecraft and missions to the Moon and Mars.

[figure 1.5.1.5a here]

[figure 1.5.1.5b here]

The propagation of galactic cosmic ions through matter has been studied by many researchers as a means of determining the origin of these ions as well as evaluation of required shielding. As the galactic cosmic components are transported through target media, their energies are attenuated via two distinct mechanisms: (1) electromagnetic interactions, resulting in ionization and excitation, and (2) nuclear interactions, resulting in the generation of a multitude of cascading secondary particles from all subsequent-generation collisions (fragmentation).

The energy is lost in extremely small increments in many collisions of electromagnetic interactions along the incident particle's path, and the average rate of energy loss per unit path length (MeV/(g/cm^2)) is expressed by the stopping power. Comprehensive tables of stopping powers versus particle energy are available in the literature (Barkas and Berger 1964; Williamson et al. 1966; Steward 1968; Janni 1966; Bichsel 1969).

For the strong nuclear interactions of the incident particle with a nucleus of the target medium, the quantum multiple scattering of heavy ion fragmentation (QMSFRG) describes the physics of the abrasion-ablation model of fragmentation (Cucinotta et al. 1992, 1997a, 1997b, 1998, Cucinotta and Dubey 1994) and agrees well with experimental data (Brechtmann and Heinrich, 1988; Webber et al., 1990b; Knott et al., 1996, 1997; Zeitlin et al., 1997, 2001). The theoretical calculation of the fragmentation cross sections involves the following areas: (1) the description of the probability of removing a given amount of mass and charge, (2) the description of the distribution of pre-fragment excitation energies formed in the abrasion step, and (3) the description of the statistical decay of the pre-fragments to form the final fragment distribution. A particular final nuclide as a result of the de-excitation of a primary residue is the nuclear fragment, sometimes referred to as a secondary product. Customarily in cosmic ion transport studies, the fragment velocities are assumed to be equal to the fragmenting ion velocity before collision at the interaction site (Wilson et al. 1993; Townsend et al. 1993).

In the last 25 years, the description of GCR transport in shielding has improved dramatically for the nuclear interactions and propagation of protons, heavy ions, and their secondaries. Major milestones include the development of an accurate free space GCR model (Badhwar and O'Neill, 1992), the HZETRN code (Wilson, 1977;Wilson et al., 1991), the measurement of a significant number of fragmentation cross sections (Brechtmann and Heinrich, 1988; Webber et al., 1990b, 1998; Knott et al., 1996, 1997; Zeitlin et al., 1997, 2001), and the development of an accurate nuclear fragmentation model (Cucinotta et al., 1997b, 1998).

Laboratory (Schimmerling et al., 1989) and spaceflight (Badhwar and Cucinotta, 2000) validation data have also become available. The combination of the GCR model of Badhwar and O'Neill, QMSFRG cross section data base, and HZETRN transport code have been shown to agree with flight measurements of GCR dose and dose equivalent within ±15% on several space vehicles (Cucinotta et al. 2006b). However, further spectral data sets, both in space and at heavy ion accelerators, are needed to fully validate these codes.

The implementation of heavy ion transport models has progressed from models that did not satisfy unitarity (Letaw et al. 1983), to the current fully energy-dependent models with accurate absorption cross sections (Shinn et al., 1994; Wilson et al., 1993b; Cucinotta, 1993). Future work may still be required for light-particle transport (n, p, d, t, h, α, and mesons and their decays), including establishing production cross section models and data, and understanding the role of angular deflections, which are more important for neutrons than for heavy ion transport. However, the heavy ion problem is in much better shape with many of the remaining tasks of implementation. One exception may be improvements in fragmentation cross sections and laboratory validation for Z=1–5 nuclei produced from the heavier projectile nuclei (Z >10).

c) Trapped Radiation Belts

All of the magnetized planets have populations of highly energetic particles that are trapped in the planetary magnetic fields. The most extensively studied of these trapped populations are Earth's radiation belts (the Van Allen belts) and the radiation belts of Jupiter. The magnetic field surrounding the Earth is roughly in a dipole configuration and charged particles are trapped in the geomagnetosphere (Van Allen et al. 1958), where there are two geomagnetically trapped radiation belts with high radiation intensities. The stable trapped radiation in inner zone, consisting mostly of protons with a small percentage of electrons, is primarily centered at an altitude of 2,000 km; and the transient outer zone, consisting mostly

of low-energy electrons with a small percentage of protons, at 20,000 km (Parker and West 1973). Energies range from ~ 100 keV to > 400 MeV for protons and from 10s of keV to > 10 MeV for electrons. The particles undergo three distinct motions: (1) a spiralling around the magnetic field lines in a helical motion having typical spiralling period of 10^{-6} seconds for electrons and 10^{-3} seconds for protons; (2) a bouncing back and forth along the field lines between mirror points having typical bounce period of 0.1-2 seconds depending on energy and particle; (3) a drifting around the Earth with typical drift period of 1-10 hours for electrons and 5 seconds-30 minutes for protons depending on energy. These naturally trapped Van Allen belts in a plane normal to the solar wind direction are spatially distorted by the solar wind pressing on the geomagnetosphere.

The Earth's magnetic field is not centered at the Earth's geographic center, and the main dipole moment, along the principal axis of the magnetic filed, is tilted with respect to the Earth's rotational axis. Thus, the geomagnetic filed is not symmetrical with respect to geographic coordinates. An interesting combination of two geomagnetic features, (1) the effective dipole displaced away from Brazil, and (2) the local distortion of geomagnetic field in South Africa called Capetown anomaly, causes trapped particles of the inner belt to dip close to the surface of the Earth in the region of the South Atlantic Ocean between Brazil and South Africa. This increase of particle flux at low altitude has been called the South Atlantic anomaly (SAA). The most radiation encountered by satellites in low-inclination orbits comes from the SAA.

Manned missions at low Earth orbit (LEO) are flown at altitudes below the inner belt. But, the 51.6° inclination orbit, such as the International Space Station (ISS), takes high geomagnetic latitudes where the exposures to the increased relativistic electron in the radiation belt and SPE fluxes during major solar disturbances are unavoidable as well as the higher GCR fluxes. Reduction of radiation risk at ISS orbit can be relatively easy and recommendations can be found in National Research Council (NRC) report (2000). However, astronauts embarking on

or returning from journeys to the Moon or Mars will have to pass through the Van Allen belts and will be exposed for brief periods to high levels of radiation.

1.5.1.2 Space Radiation Protection Issues

NASA follows radiation exposure limits for humans in space (Cucinotta and Durante, 2006) and implements appropriate risk mitigation measures in order to ensure that humans can safely live and work in the space radiation environment, anywhere, anytime. In the context of the radiation protection principle of as low as reasonable achievable (ALARA), "safely" means that acceptable risks are not exceeded during crew members' lifetimes, where "acceptable risks" include limits on post-mission and multi-mission consequences. The most important radiations for biological considerations are the trapped protons in the inner zone, the trapped electrons in both the inner and the outer zones, SPEs, and especially GCR (Wilson et al. 1991).

The more intense components of space radiations such as SPEs and trapped radiation were considered to be the principal radiation hazards for the past short duration exploratory missions, since the continuous GCR background exposures are of low intensity. In the past, career radiation limits were based on fatal cancer risks, and increased lifetime cancer risk above the natural incidence is limited within 3 percent in NASA missions at LEO as recommended by the National Council on Radiation Protection and Measurements (NCRP, 2000).

Safety concerns for long term space explorations include carcinogenesis, degenerative tissue effects, such as cataracts (Cucinotta et al. 2001) or heart diseases (Preston et al. 2003; Howe et al. 2004; Yang and Ainsworth 1982), and acute radiation syndromes (NCRP 2000). Other risks, such as damage to the central nervous system (CNS), are a concern for HZE nuclei (NAS 1996), because of their unique pattern of energy deposition on the microscopic scale of

living cells. Although standards for lunar missions are under review at this time, it is expected that cancer risks will be the major component of radiation limits, however new knowledge on chronic non-cancer risks from radiation is needed.

Because the abundance of some heavy ions from major SPEs may increase rapidly by 3 or 4 orders of magnitude above GCR background for periods of several hours to days, SPEs present the most significant risk for short-stay lunar missions (<90 d). The primary radiation protection from SPE is to control early somatic radiation effects, which may impact mission safety. However, effective mitigation against SPEs is viable by implementing several options: a spacecraft devised by high-performance structural material with effective radiation shielding properties, such as carbon composite with high hydrogen content; adequate mission planning for timing and location; and seeking a shelter and using personal localized shielding in timely manner with the warning system developed (Cucinotta et al. 2006). It has been assessed that acute death is extremely unlikely from any known large SPE, and acute radiation sickness extremely improbable inside exploratory spacecraft or lunar habitation module except EVA performed during major SPE for greater than 2 hours (Cucinotta, 2006a). Skin damage (Kim et al. 2006) and cataracts (Cucinotta et al. 2001) are specially concerned due to the dose rate effect.

In contrast, for long-term missions, such as long duration lunar (>90 d) or Mars missions, risk from GCR may exceed the acceptable radiation risk limits. The unusually high specific ionization of HZE nuclei of GCR will be the ultimate limiting factor in long-term space operations, because their relative dose contributions are comparable to those of light particles but their biological effects, which are yet poorly understood, are far more serious (Cucinotta and Durante 2006).

For the effort of accurate projections of radiation doses to astronauts, which are required for space mission planning on future exploratory class and long-duration missions (Cucinotta and

Durante 2006), a solar cycle statistical model has been developed (Wilson et al. 1999; Kim and Wilson 2000; Kim et al. 2004, 2006d). A systematic method of making short-range projections of future levels of solar cycle activity was established by quantifying the progression level of sunspot numbers within the solar cycle. The resultant solar activity levels were coupled to GCR deceleration potential (ϕ) and the mean occurrence frequency of SPEs (ν) for the projection of future space radiation environment, which is interest in radiation protection.

The GCR deceleration parameter, $\phi(t)$, represents the temporal GCR environment in interplanetary space, and the calculated values are shown as a function of time in the upper graph of figure 1.5.1.6. The point dose equivalents inside a typical equipment room of a spacecraft (5 g/cm^2 aluminum) are calculated from the GCR environment in interplanetary space, that is determined as a function of $\phi(t)$, and at LEO by using the HZETRN code system (Wilson et al 1995) as shown in the lower graph of figure 1.5.1.6. This calculation shows that within the simple and representative spacecraft configuration the GCR exposure levels are simply affected by the solar modulation in interplanetary space by a factor of three, while at LEO to about a factor of two due to the further modification of the GCR environment by geomagnetic fields and atmospheric shielding.

[figure 1.5.1.6 here]

Although no definite pattern of SPE occurrences has been observed in the past solar cycles, large SPEs have been recorded during the solar active years as shown in figure 1.5.1.7. This strong possibility of large SPE occurrences at high $\phi(t)$ and the multiple annual occurrences of medium to large SPEs per year during the solar active years in future cycles as shown in figure 1.5.1.8 are definitively major operational problems in planning and protecting

astronauts on future missions to the moon and Mars. Since the sporadic nature of SPEs makes it impossible
to pinpoint the exact time of future large SPE occurrences, the probabilities of SPEs occurring in a short mission period and the exposure levels from various SPEs are calculated in figure 1.5.1.9 for guidance in the design of protection systems.

[figure 1.5.1.7 here]

[figure 1.5.1.8 here]

[figure 1.5.1.9 here]

1.5.1.3 Summary

Considerable effort and improvement have been made in the study of ionizing radiation exposure occurring in various regions of space. Satellites and spacecrafts equipped with innovative instruments are continually refining particle data and providing more accurate information on the ionizing radiation environment. The major problem in accurate spectral definition of ionizing radiation appears to be the detailed energy spectra, especially at high energies, which is important parameter for accurate radiation risk assessment. Magnitude of risks posed by exposure to radiation in future space missions is subject to the accuracies of predictive forecast of event size of SPE, GCR environment, geomagnetic fields, and atmospheric radiation environment. Although heavy ion fragmentations and interactions are adequately resolved through laboratory study and model development, improvements in fragmentation cross sections for the light nuclei produced from HZE nuclei and their laboratory validation are still required to achieve the principal goal of planetary GCR simulation at a critical exposure site. More accurate prediction procedure for ionizing radiation environment can be made with a better understanding of the solar and space physics,

fulfillment of required measurements for nuclear/atomic processes, and their validation and verification with spaceflights and heavy ion accelerators experiments. It is certainly true that the continued advancements in solar and space physics combining with physical measurements will strengthen the confidence of future manned exploration of solar system. Advancements in radiobiology will surely give the meaningful radiation hazard assessments for short and long term effects, by which appropriate and effective mitigation measures can be placed to ensure that humans safely live and work in the space, anywhere, anytime.

References

Adams, J. H., Silberberg, R., Tsao, C. H., 1981. *Cosmic ray effects on microelectronics*. Part I- the near-earth particle environment. NRL Memo. Rep. 4506-pt. I, U.S. Navy.

Badhwar, G. D., 1999. Radiation dose rates in Space Shuttle as a function of atmospheric density. *Radiat. Meas*., **30**, pp. 401-414.

Badhwar, G.D., Cucinotta, F.A., 2000. A comparison on depth dependence of dose and linear energy transfer spectra in aluminum and polyethylene. Radiat. Res. **153**, pp. 1–8.

Badhwar, G. D. and O'Neill, P. M., 1992. An improved model of GCR for space exploration missions. *Nucl. Tracks Radiat. Meas.*, **20**, pp. 403-410.

Barkas, W. H. and Berger, M. J., 1964. Tables of energy losses and ranges of heavy charged particles, in Studies in penetration of charged particles in matter, NAS-NRC Publ. 1133, pp. 103-172. Nat. Acad. of Sci.- Nat. Res. Council Publ., Washington, D.C.

Bertsch, D. L., Fichtel, C.E., Reames, D. V., 1969. Relative abundance of iron-group nuclei in solar cosmic rays. *Astrophys. J.*, **157**, pp. L53-L56.

Bichsel, H., 1969. Passage of charged particles through matter. Univ. of Southern California Publ. USC-136-150.

Biswas, S., Fichtel, C.E., Guss, D.E., 1962. Study of the hydrogen, helium, and heavy nuclei in the November 12 1960 Solar Cosmic-Ray Event. Phys. Rev. 128 (6), 2756–2771.

Biswas, S., Fichtel, C.E., Guss, D.E., 1966. Solar cosmic-ray multiply charged nuclei and the July 18, 1961, solar event. *J. Geophys. Res.*, **71**, pp. 4071-4077.

Biswas, S., Fichtel, C.E., Guss, D.E., Waddington, C. J., 1963. Hydrogen, helium and heavy nuclei from the solar event on November 15, 1960. *J. Geophys. Res.*, **68**, pp. 3109-3122.

Bobcock, H. W., 1961. The topology of the Sun's magnetic field and the 22-year cycle. *Astrophys. J.*, **133**(2), pp. 572-587.

Brechtmann, C., Heinrich, W., 1988. Fragmentation cross-sections of 32S at 0.7, 1.2, and 200 GeV/nucleon. Z. Phys. **A331**, 463–472.

Colgate, S. A., Grasberger, W. H., White, R. H., 1963. The dynamics of a supernova explosion. *J. Phys. Soc. Japan*, **17**, Suppl. A-III, p. 157.

Cucinotta, F.A., 1993. Calculations of cosmic-ray helium transport in shielding materials. NASA TP-3354.

Cucinotta, F. A., Dubey, R. R., 1994. Alpha cluster description of excitation energies in $^{12}C(^{12}C, 3\ \alpha)X$ at 2.1 GeV, *Phys. Rev.,* **C50**, pp. 979-984.

Cucinotta, F. A., Townsend, L. W., Wilson, J. W., 1992. Multiple scattering effects in quasi-elastic a-4He scattering. *Phys. Rev.,* **C46**, pp. 1451-1456.

Cucinotta, F. A., Wilson, J. W., Shinn, J. L., Tripathi, R. K., Maung, K. M., Badavi, F. F., Katz, R., Dubey, R. R., 1997a. Computational procedures and database development, In: Wilson, J. W., Miller, J., Konradi, A., Cucinotta, F. A. (Eds.), NASA workshop on shielding strategies for human space exploration. NASA CP-3360.

Cucinotta, F. A., Wilson, J. W., Townsend, L. W., 1997b. Abraison-ablation model for neutron production in heavy ion collisions, *Nucl. Phys.* **A619**, pp. 202-212.

Cucinotta, F. A., Wilson, J. W.,Tripathi, R. K., Townsend, L. W., 1998. Microscopic fragmentation model for galactic cosmic ray studies, *Adv. Space Res.*, **22**, pp. 533-537.

Cucinotta, F. A., Wilson, J. W., Williams, J. R., Dicello, J. F., 2000. Analysis of Mir-18 results for physical and biological dosimetry: Radiation shielding effectiveness in LEO, *Radiat. Meas.*, **32**, pp. 181-191.

Cucinotta, F. A., Manuel, F. K., Jones, J., Iszard, G., Murrey, J., Djojonegro, B., Wear, M., 2001. Space radiation and cataracts in astronauts. *Radiat. Res.*, **156**, pp. 460-466.

Cucinotta, F. A., Durante, M., 2006. Cancer risk from exposure to galactic cosmic rays: implications for space exploration by human beings, *Lancet Oncology*, **7**, pp. 431-435.

Cucinotta, F. A., Kim, M. Y., Ren, L., 2006a. Evaluating shielding effectiveness for reducing space radiation cancer risks. *Radiat. Meas.*, **41**, pp. 1173-1185.

Cucinotta, F. A., Wilson, J. W., Saganti, P., Hu, X., Kim, M. Y., Cleghorn T., Zeitlin C., Tripathi, R.K., 2006b. Isotopic dependence of GCR fluence behind shielding. *Radiat. Meas.*, **41**, pp. 1235-1249.

Fields, B.D., Olive, K.A., Schramm, D.N., 1994. Cosmic ray models for early galactic lithium, beryllium and boron production. Fermilab-Pub-94/010-A.

Forbush, S. E., 1937. On the effects in cosmic-ray intensity observed during the recent magnetic storm, *Phys. Rev.* **51**, pp. 1108-1109.

Freier, P.S., 1963. Emulsion measurements of solar alpha particles and protons, *J. Geophys. Res.*, **68**, pp. 1805-1810.

Freier, P.S., Webber, W.R., 1963. Exponential rigidity spectrums for solar-flare cosmic rays. *J. Geophys. Res.* **68**, 1605–1629.

Ginzburg, V. L., 1958. The origin of cosmic radiation. *Progr. Elem. Particle Cosmic Ray Phys.*, **4**, p. 339.

Goswami, J. N., McGuire, R. E., Reedy, R. C., Lal, D., and Jha, R., 1988. Solar flare protons and alpha particles during the last three solar cycles, *J. Geophys. Res.*, **93**(A7), pp. 7195-7205.

Haffner, J. W., 1967. *Radiation and Shielding in Space*. Nuclear Science and Technology, Series 4, Academic Press.

Hesse, A., et al., 1991. The isotopic composition of silicon and iron in the cosmic radiation as measured by the ALICE experiment. 22nd International Conference, The Dublin Institute for Advanced Studies, Dublin, pp. 596–599.

Howe, G. R., Zablotska, L. B., Fix, J. J., Egel, J., Buchanan, J., 2004. Analysis of the motality experience amongst U.S. nuclear power industry workers after chronic low-dose exposure to ionizing radiation. *Radiat. Res.*, **162**, pp. 517-526.

Janni, J. F., 1966. Calculations of energy loss, range path length, straggling, multiple scattering, and the probability of inelastic nuclear collisions for 0.1 to 1000 MeV protons. Air Force Weapons Lab. Rept. NWL-TR-65-150.

Kim, M. Y., Wilson, J. W., 2000. *Examination of solar cycle statistical model and new prediction of solar cycle 23*, NASA/TP-2000–210536.

Kim, M. Y., Wilson, J. W., Cucinotta, F. A., 2004. *An improved solar cycle statistical model for the projection of near future sunspot cycles*, NASA/TP-2004–212070.

Kim, M. Y., Hu, X., Cucinotta, F. A., 2005. Effect of shielding materials from SPEs on the lunar and Mars surface, AIAA 2005-6653.

Kim, M. Y., Cucinotta, F. A., Wilson, J. W., 2006a. Mean occurrence frequency and temporal risk analysis of solar particle events. *Radiat. Meas.*, **41**, pp. 1115-1122.

Kim, M. Y., Cucinotta, F. A., Wilson, J. W., 2006b. A temporal forecast of radiation environments for future space exploration missions, *Radiat. Environ Biophy.*, DOI 10.1007/s00411-006-0080-1 (online first).

Kim, M. Y., George, K. A., Cucinotta, F. A., 2006c. Evaluation of skin cancer risk for lunar and Mars missions, *Adv. Spa. Res.*, **37**, pp. 1798-1803.

Kim, M. Y., Wilson, J. W., Cucinotta, F.A., 2006d. A solar cycle statistical model for the projection of space radiation environment. *Adv. Spa. Res.* **37**, pp. 1741–1748.

King, J. H., 1972. Unpublished records of a NASA workshop held several weeks after the August 1972 event, correspondence dated October 24, 1972, from J.H. King at NASA Goddard Space Flight Center to A.C. Hardy at NASA Johnson Space Center.

Knott, C.N., et al., 1996. Interactions of relativistic neon to nickel projectiles in hydrogen, elemental production cross-sections. Phys. Rev. C **53**, 347–357.

Knott, C.N., et al., 1997. Interactions of relativistic 36Ar and 40Ar nuclei in hydrogen: isotopic production cross-sections. Phys. Rev. C **56**, 398–406.

Kundu, M. R., and Haddock, F. T., 1960. A relation between solar radio emission and polar cap absorption of cosmic noise. *Nature* **186**, pp. 610-613.

Letaw, J., Tsao, C.H., Silberberg, R., 1983. Matrix methods of cosmic ray propagation. In: Shapiro, M.M. (Ed.), Composition and Origin of Cosmic Rays. D. Reidel Publ. Co, pp. 337–342.

Lukasiak, A., Ferrando, P., McDonald, F.B., Webber, W.R., 1993. Cosmic ray composition of $6<Z<8$ nuclei in the energy range 50-150 MeV/n by the Voyager spacecraft during the solar minimum and maximum periods. 23rd International Cosmic Ray Conference, La Jolla, USA, pp. 539–542.

Lukasiak, A., McDonald, F.B., Webber, W.R., Ferrando, P., 1995. Voyager measurements of the isotopic composition of Sc, Ti, V, Cr, Mn, and Fe nuclei. 24th International Conference Ray Conference, vol. 2, pp. 576–579.

McCracken, K. G., Dreschhoff, G., Zeller, E. J., et al., 2001. Solar cosmic ray events for the period 1561–1994 1. Identification in polar ice, 1561–1950. J Geophys Res **106** (A10), pp. 21585–21598.

Meyer, P., 1969. Cosmic rays in the galaxy. *Ann. Rev. Astron. Astrophys.*, **7**, p. 1.

National Academy of Sciences (NAS), 1996. National Academy of Sciences Space Science Board, Report of the task group on the biological effects of space radiation, Radiation hazards to crews on interplanetary mission, Washington, D.C.

National Council on Radiation Protection and Measurements (NCRP), 2000. Radiation protection guidance for activities in low-Earth orbit. NCRP Report No. 132, Bethesda, MD.

National Geophysical Data Center (NGDC): GOES Space Environment Monitor (SEM) data, 2006. NOAA, http://goes.ngdc.noaa.gov/data/, Accessed December 20, 2006.

NRC (National Research Council). 2000. *Radiation and the International Space Station: Recommendations to Reduce Risk.* National Academy Press, Washington D.C.

Parker, E.N., 1965. The passage of energetic charged particles through interplanetary space. *Planet Space Sci.*, **13**, pp. 9–49.

Parker, E.N., West, V. R., 1973. Bioastronautics data book, NASA SP-3006, National Technical Information Service, Springfield, VA.

Preston, D. L., Shimizu, Y., Pierce, D. A., Suyumac, A., Mabuchi, K., 2003. Studies of motality of atomic bomb survivors, Report 13: Solid cancer and noncancer disease motality: 1950-1977, *Radiat. Res.*, **160**, pp. 381-407.

Schimmerling, W., Miller, J., Wong, M., Rapkin, M., Howard, J., Spieler, H.G., Blair, J.V., 1989. The fragmentation of 670AMeV neon-20 as a function of depth in water. Radiat. Res. 120, 36–51.

Shea, M. A., Smart, D. F., 1990. A summary of major proton events. *Solar Phys* **127**, pp. 297–320.

Shinn, J.L., Wilson, J.W., Badavi, F.F., 1994. Fully-energy dependent HZETRN. NASA TP-3243.

Simpson, J. A., 1983. Introduction to the galactic cosmic radiation. In M. Shapiro, ed. *Composition and origin of cosmic rays.* D. Reidel Publ. Co., 1983, pp. 1-24.

Simpson, J. A., 1983b. Elemental and isotropic composition of the galactic cosmic rays. In J. Jackson, H. Gove, R. Schwitters, eds. *Annual review of nuclear and particle science*. **33**, Annual Reviews Inc., 1983, pp. 323-381.

Steward, P. G., 1968. Stopping power and range for any nucleus in the specific energy interval 0.01- to 500 MeV/amu in any non-gaseous material. Univ. of California Radiat. Lab. Rep. UCRL 18127.

Townsend, L. W., Wilson, J. W., Tripathi, R. K., Norbury, J. W., Badavi, F. F., Khan, F., 1993. An energy-dependent semiempirical nuclear fragmentation model, NASA TP-3310.

Van Allen, J. A., Ludwig, G. H., Ray, E. C., McIllwain, C. E., 1958. Observation of high intensity radiation by satellites 1958 Alpha and Gamma, *Jet Propul.*, **28**, pp. 588-592.

Webber, W.R., Kish, J.C., Schrier, D.A., 1985. Cosmic ray isotope measurements with a new cerenkov total energy telescope. 19th International Cosmic Ray Conference, La Jolla, USA, pp. 88–95.

Webber, W.R., Southoul, A., Ferrando, P., Gupta, M., 1990a. The source charge and isotopic abundances of cosmic rays with $Z = 9–16$: a study using new fragmentation cross-sections. *Astrophys. J.* **348**, 611–620.

Webber, W.R., Kish, J.C., Schrier, D.A., 1990b. Individual isotopic fragmentation cross-sections of relativistic nuclei in hydrogen, helium and carbon targets. Phys. Rev. C **41**, 547.

Webber, W.R., et al., 1998. Measurements of charge changing and isotopic cross sections at 600MeV/nucleon from the interactions of 30 separate beams at relativistic nuclei from 10B to 55Mn in a liquid hydrogen target. Phys. Rev. C **58**, 3539–3552.

Wiedenback, M.E., 1985. The isotopic composition on cosmic ray chlorine. 19th International Cosmic Ray Conference, La Jolla, USA, pp. 84–87.

Wiedenback, M.E., Greiner, D.E., 1981. High-resolution observations of the isotopic composition of carbon and silicon in the galactic cosmic rays. Astrophys. J. 247, L119–L122.

Williamson, C. F., Boujot, J. P., Picard, J., 1966. Tables of ranges and stopping power of chemical elements for charged particles of energy 0.05 to 500 MeV, Rep. CEA-R3042. Centre d'Etudes Nucleaires de Saclay, Saclay, France.

Wilson, J.W., 1977. Analysis of theory of high-energy transport. NASA TN D-8381.

Wilson, J. W., Townsend, L. W., Schimmerling, W., Khandelwal, G. S., Khan, F., Nealy, J. E., Cucinotta, F. A., Simonsen, L. C., Shinn, J. L., Norbury, J. W., 1991. *Transport methods and interactions for space radiations*, NASA RP-1257, National Technical Information Service, Springfield, VA.

Wilson, J. W., Chun, S. Y., Badavi, F. F., John, S., 1993. Coulomb effects in low-energy nuclear fragmentation, NASA TP-3352.

Wilson, J.W., Thibeault, S.A., Nealy, J.E., Kim, M.Y., Kiefer, R.L., 1993b. Studies in space radiation shield performance. Proceedings of the Engineering & Architecture Symposium, Prairie View A&M Univ., pp. 169–176.

Wilson, J. W., Kim, M., Schimmerling, W., Badavi, F. F., Thibeault, S. A., Cucinotta, F. A., Shinn, J. L., and Kiefer, R., 1995. Issues in space radiation protection, *Health Physics*, **68**, pp. 50-58.

Wilson, J. W., Badavi, F. F., Cucinotta, F. A. et al., 1995. HZETRN: description of a free-space ion and nucleon transport and shielding computer program. NASA TP-3495.

Wilson, J. W., Cucinotta, F. A., Shinn, J. L., Simonsen, L. C., Dubey, R. R., Jordan, W. R., Jones, T. D., Chang, C. K., Kim, M. Y., 1999. Shielding from solar particle event exposures in deep space *Radiat. Meas.*, **30**, pp. 361-382.

Wilson, J. W., Kim, M. Y., Shinn, J. L., Tai, H., Cucinotta, F. A., Badhwar, G. D., Badavi, F. F., Atwell, W., 1999. *Solar cycle variation and application to the space radiation environment*, NASA/TP-1999–209369.

Xapsos MA, Barth JL, Stassinopoulos et al., 2000. Characterizing solar proton energy spectra for radiation effects applications. IEEE Trans Nucl Sci **47**(6) pp. 2218–2223.

Yang, V. V., Ainsworth, E. J., 1982. Late effects of heavy charged particles on the fine structure of the mouse coronary artery. *Radiat. Res.*, **91**, pp. 135-144.

Zeitlin, C., Heilbronn, L., Miller, J., Rademacher, S.E., Borak, T., Carter, T.R., Frankel, K.A., Schimmerling, W., Stronach, C.E., 1997. Heavy fragment production cross-sections from 1.05 GeV/nucleon 56Fe in C, Al, Cu, Pb, and CH2 target. Phys. Rev. C **56**, 388–397.

Zeitlin, C., Fukumura, A., Heilbronn, L., Iwata, Y., Miller, J., Murakami, T., 2001. Fragmentation cross-sections of 600 MeV/nucleon 20Ne on elemental targets. Phys. Rev. C **64**, 24902.

Zeitlin, C., Cleghorn, T., Cucinotta, F., Saganti, P., Andersen, V., Lee, K., Pinsky, L., Atwell, W., Turner, R., Badhwar, G., 2004. Overview of the martian radiation environment experiment. Adv. Space Res. 33, 2204–2210.

Table 1.5.1.1 Large SPEs during Solar Cycles 19-23 with $\Phi_{30} > 10^9$ protons/cm^2

Solar Cycle	SPE	Φ_{30}, protons/cm^2
19	11/12/1960	9.00×10^9
20	8/2/1972	5.00×10^9
22	10/19/1989	4.23×10^9
23	7/14/2000	3.74×10^9
23	10/26/2003	3.25×10^9
23	11/4/2001	2.92×10^9
19	7/10/1959	2.30×10^9
23	11/8/2000	2.27×10^9
22	3/23/1991	1.74×10^9
22	8/12/1989	1.51×10^9
22	9/29/1989	1.35×10^9
23	1/16/2005	1.04×10^9
19	2/23/1956	1.00×10^9

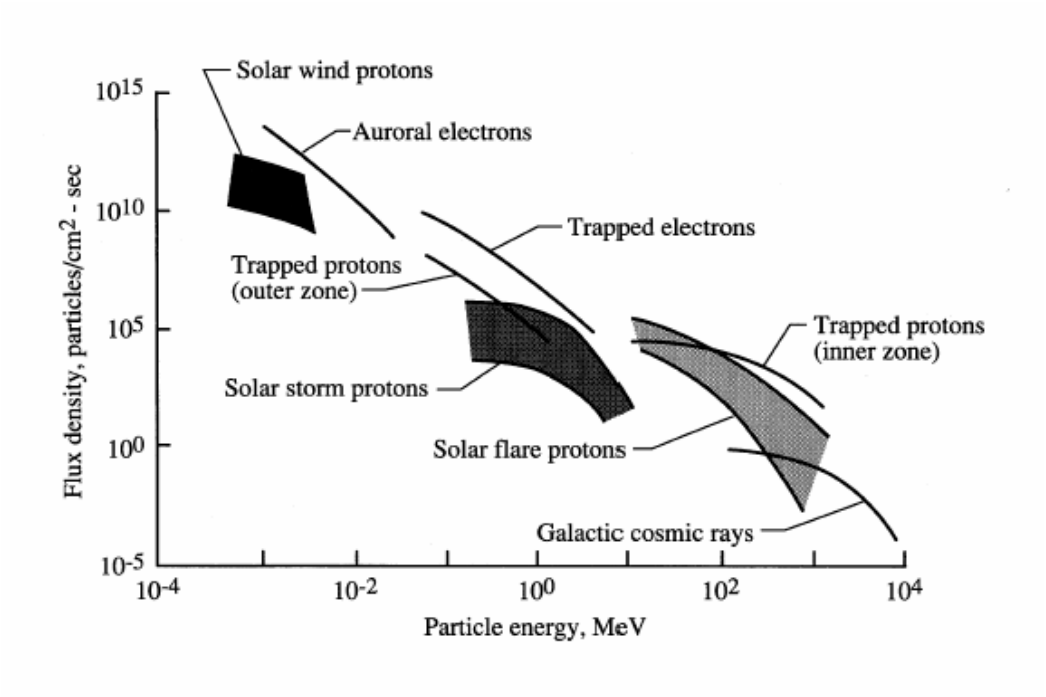

Figure 1.5.1.1. Space-radiation environment (Wilson et al. 1991)

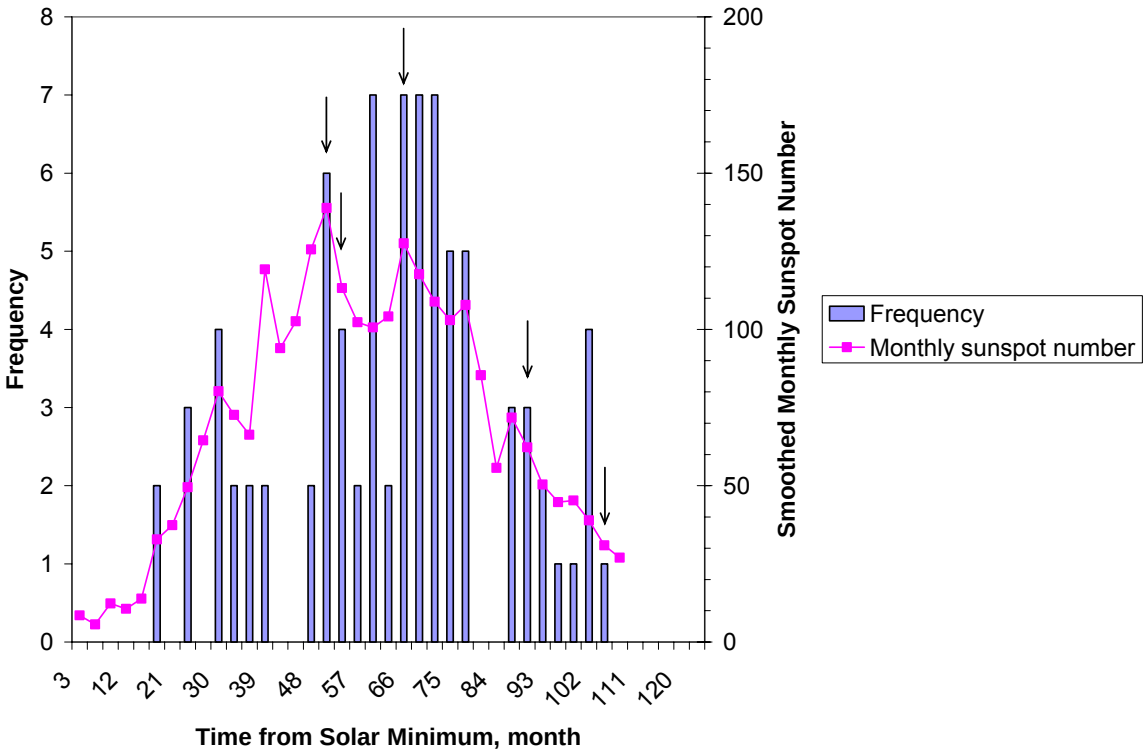

Figure 1.5.1.2. Frequency of SPE occurrence in three-month periods for solar cycle 23. The arrow indicates the occurrence time of large SPE with $\Phi_{30} > 10^9$ protons/cm^2. From left: Jul 2000, Nov 2000, Nov 2001, Oct 2003, and Jan 2005.

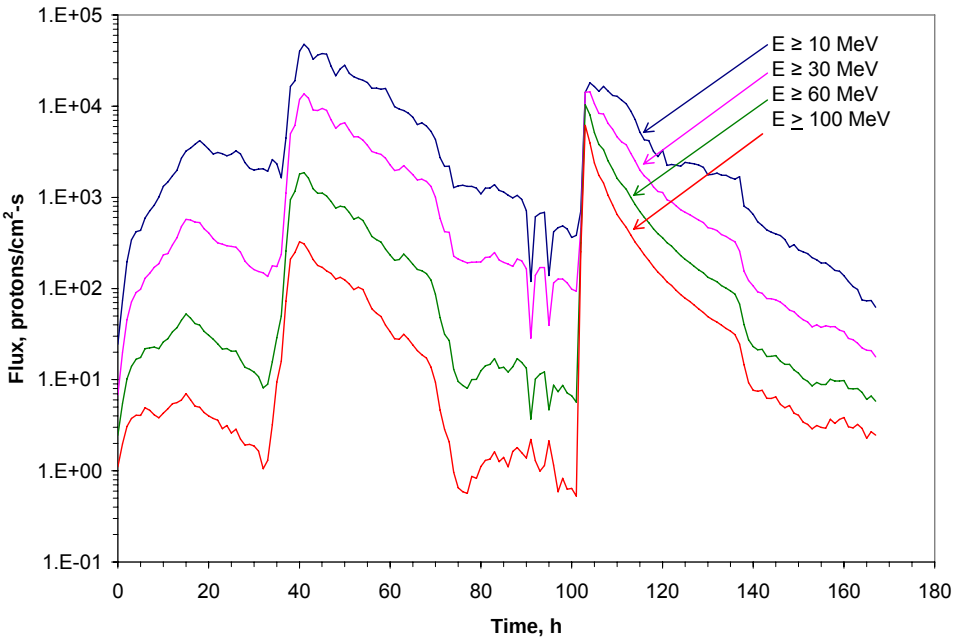

Figure 1.5.1.3. Hourly-averaged proton flux of GOES measurements during January 16-22, 2005 SPE.

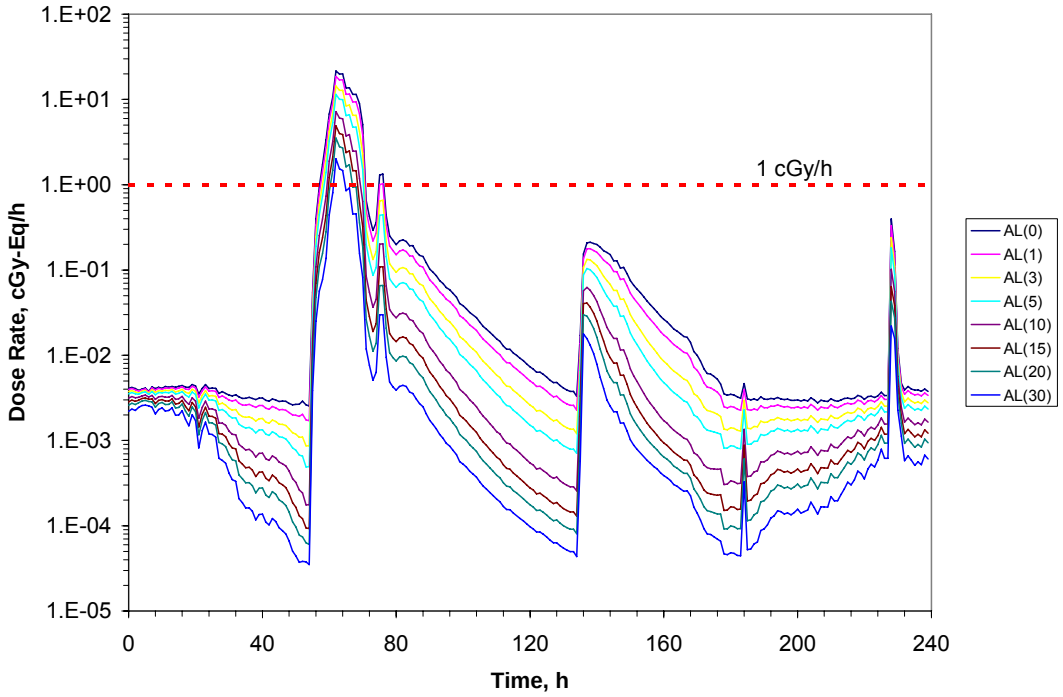

Figure 1.5.1.4a. BFO dose rate behind various aluminium thickness during August 2-11, 1972 SPE.

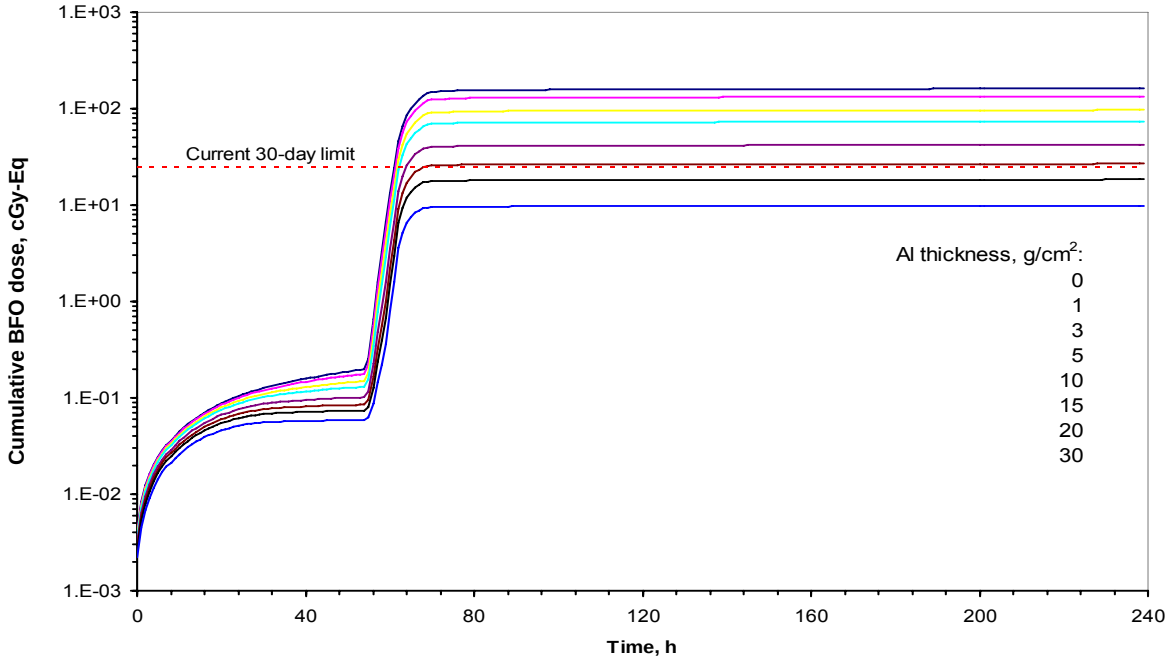

Figure 1.5.1.4b. Cumulative BFO dose behind various aluminium thickness during August 2-11, 1972 SPE.

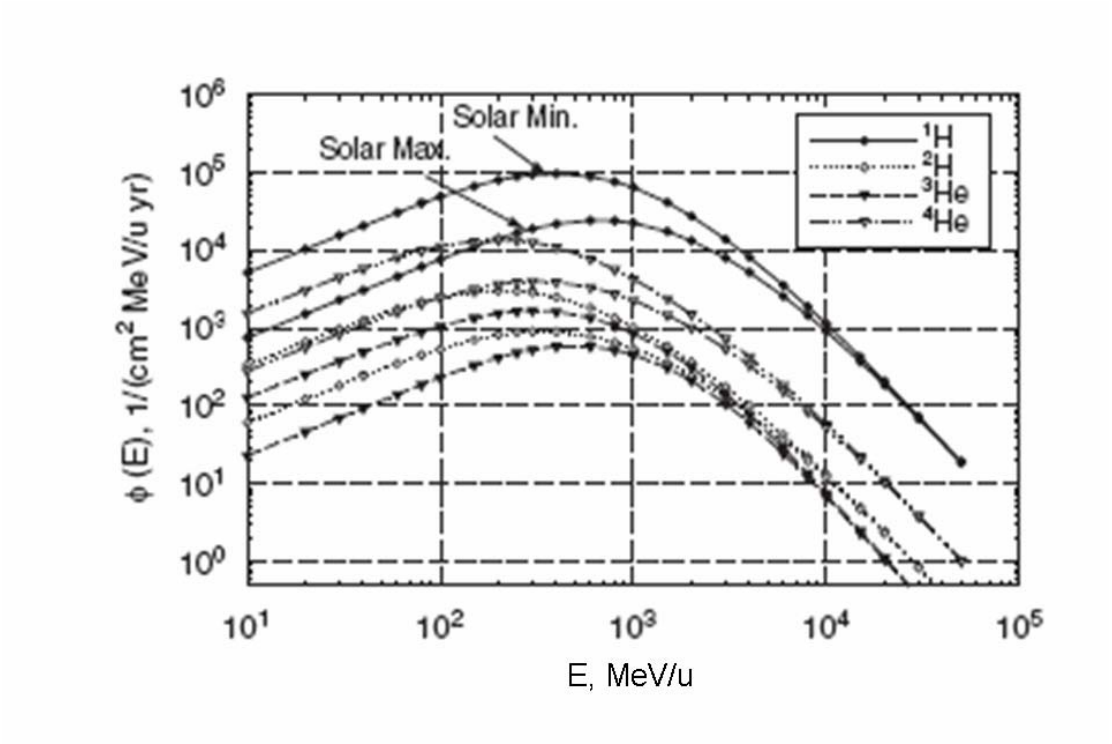

Figure 1.5.1.5a. Energy spectra for hydrogen and helium isotopes at solar minimum and solar maximum.

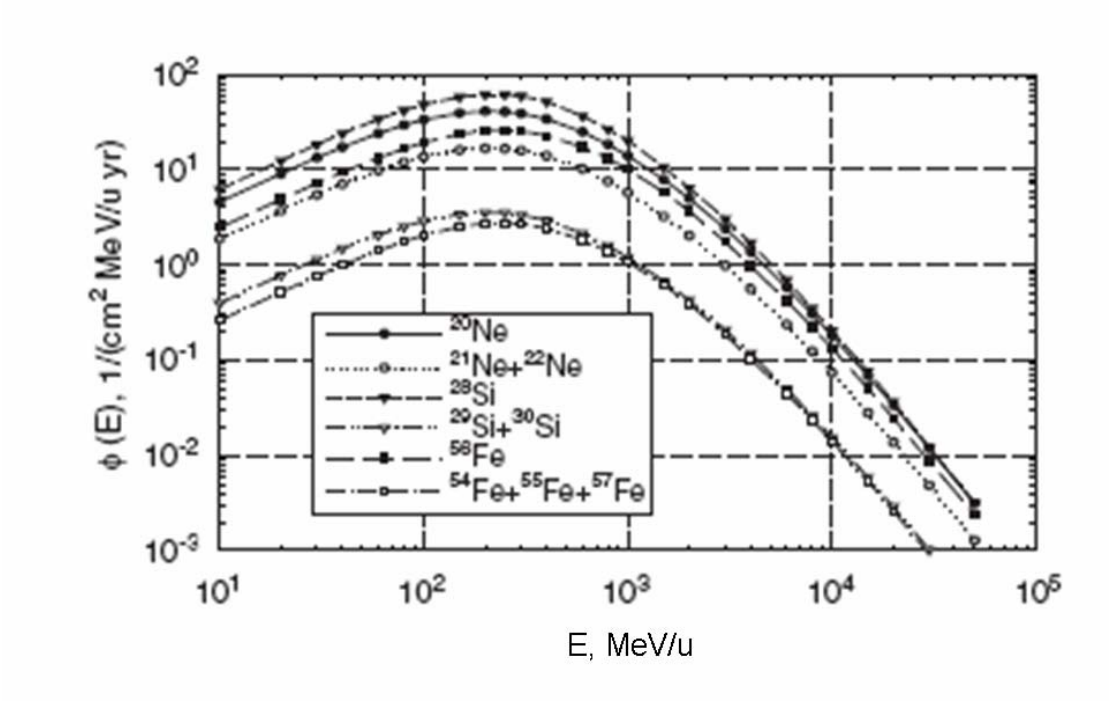

Figure 1.5.1.5b. Energy spectra for Ne, Si, and Fe isotopes at solar minimum, showing contributions from different isotopes to primary GCR composition.

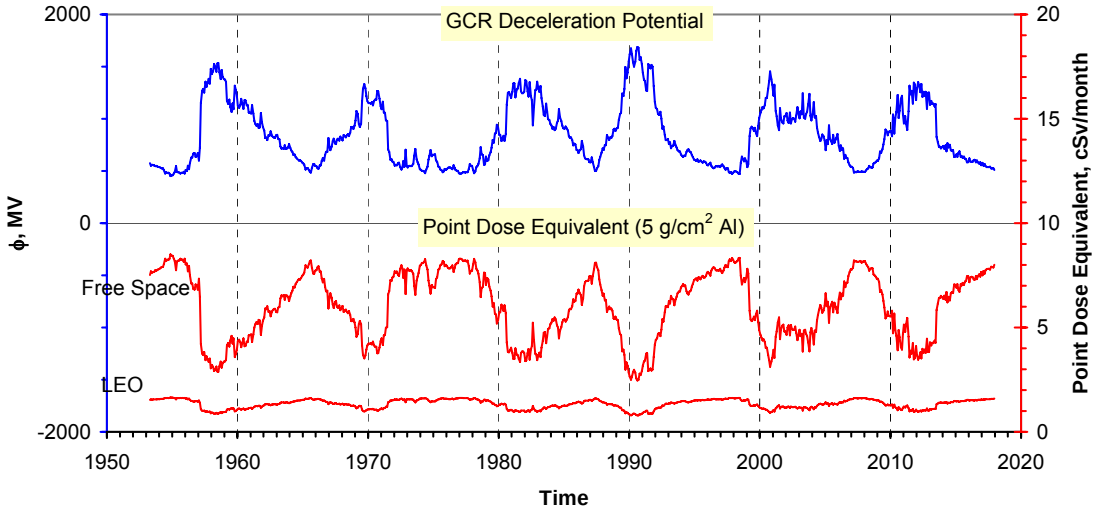

Figure 1.5.1.6. GCR deceleration parameter as a function of time (upper graph), calculated from the neutron monitor rate measurements and from the projected neutron monitor rates in future with the statistical model (Kim et al. 2006d); and point dose equivalents from the GCR inside spacecraft (lower graph), shielded with 5 g/cm^2 aluminum, calculated with HZETRN (Wilson et al. 1995).

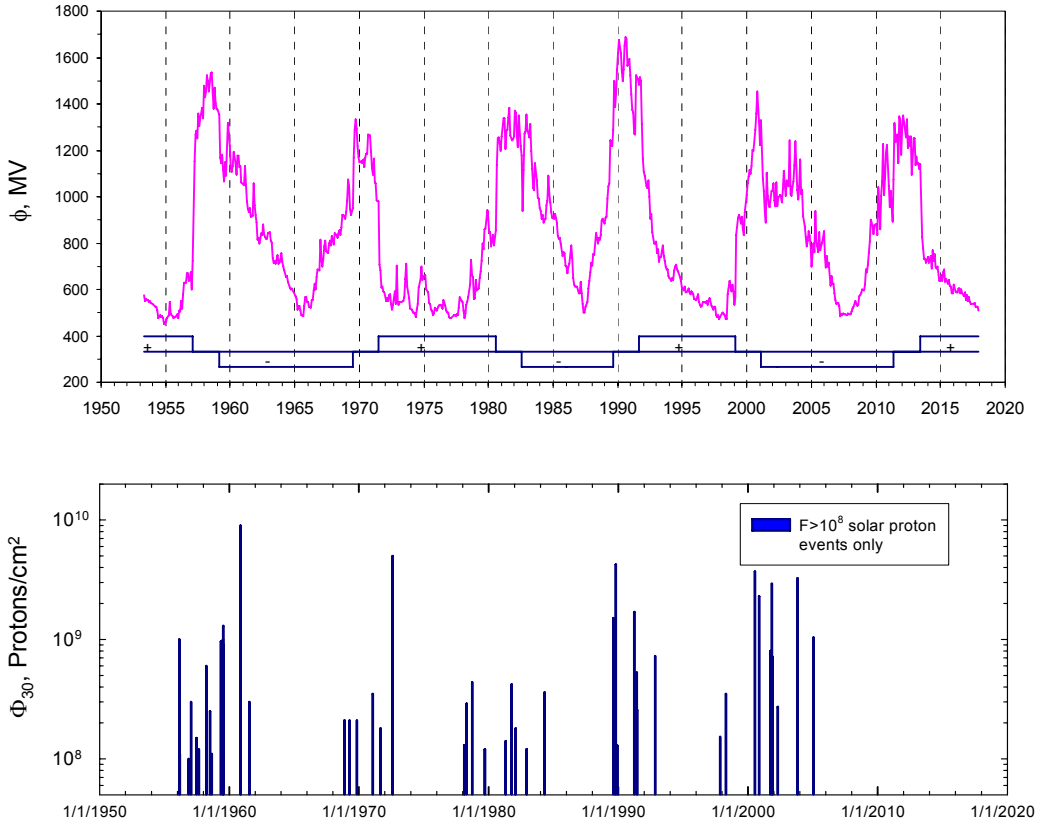

Figure 1.5.1.7. GCR deceleration parameter and large SPE occurrences (Shea and Smart 1990; NGDC 2006) (plotted for event size (Φ_{30}) > 1 × 10^8 protons/cm^2 only) as a function of time.

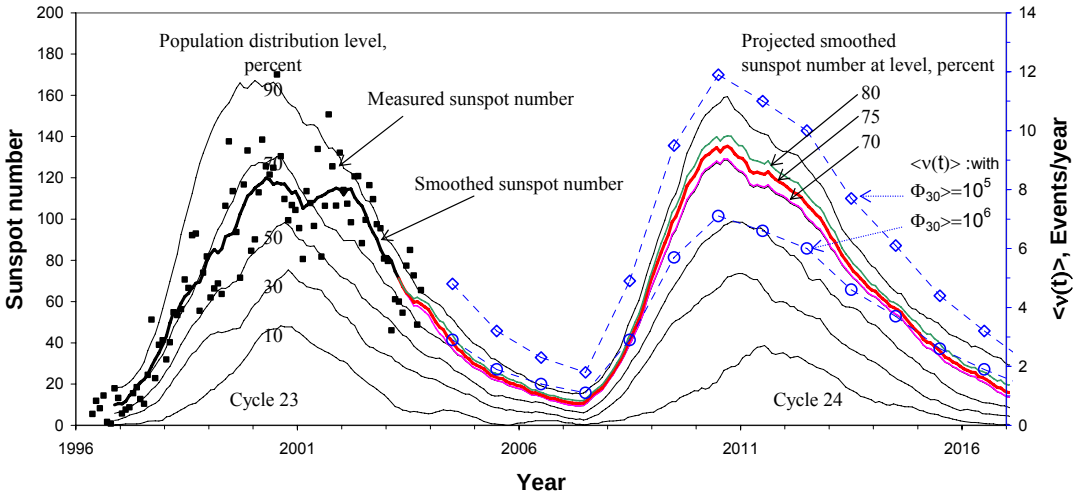

Figure 1.5.1.8. Sunspot sampling distribution and projections of solar cycles and mean occurrence frequency of SPE (Kim et al. 2006a).

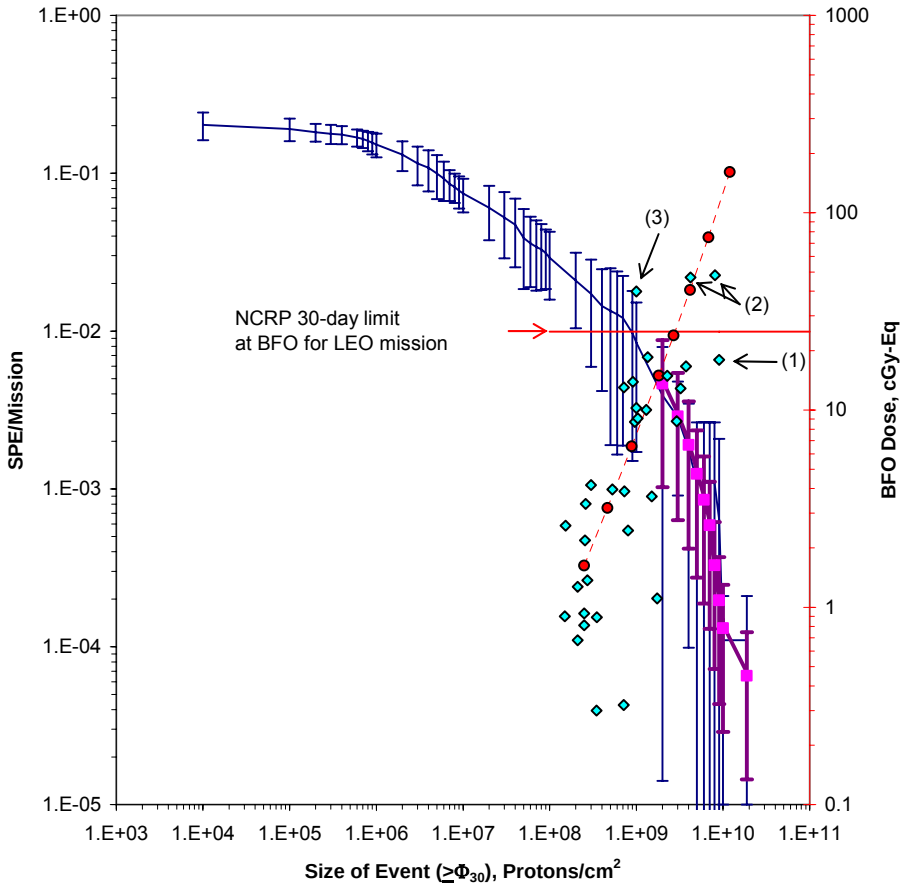

Figure 1.5.1.9. Probability of SPE in 1-week mission (thin line: average probability of SPE and statistical fluctuation during the space era; thick line: extended average probability including impulsive nitrate events (McCracken et al. 2001); filled square: impulsive nitrate events), and BFO dose inside a spacecraft of 5 g/cm^2 aluminum (line with filled circle: BFO dose of the worst-case SPE model (Xapsos et al. 2000); filled diamond: BFO dose of 34 large SPEs during the space era).

Note 1: the largest event recorded in the space era (F30); the BFO dose inside a spacecraft (5 g/cm^2 aluminum) is lower than the current NCRP limit for LEO mission (NCRP 2000).

Note 2: $\Phi_{30} > 2 \times 10^9$ protons/cm^2; the BFO dose is over the current limit.

Note 3: Φ_{30} at 70% confidence level of the worst-case SPE; the BFO dose is over the current limit.